Soft Matter

PAPER

View Article Online
View Journal | View Issue

Cite this: *Soft Matter*, 2016, 12, 6841

Orientational order and translational dynamics of magnetic particle assemblies in liquid crystals†

Stavros D. Peroukidis* and Sabine H. L. Klapp

Received 1st June 2016,
Accepted 21st July 2016

DOI: 10.1039/c6sm01264g

www.rsc.org/softmatter

Implementing extensive molecular dynamics simulations we explore the organization of magnetic particle assemblies (clusters) in a uniaxial liquid crystalline matrix comprised of rodlike particles. The magnetic particles are modelled as soft dipolar spheres with diameter significantly smaller than the width of the rods. Depending on the dipolar strength coupling the magnetic particles arrange into head-to-tail configurations forming various types of clusters including rings (closed loops) and chains. In turn, the liquid crystalline matrix induces long range orientational ordering to these structures and promotes their diffusion along the director of the phase. Different translational dynamics are exhibited as the liquid crystalline matrix transforms either from isotropic to nematic or from nematic to smectic state. This is caused due to different collective motion of the magnetic particles into various clusters in the anisotropic environments. Our results offer a physical insight for understanding both the structure and dynamics of magnetic particle assemblies in liquid crystalline matrices.

1 Introduction

Self assembly of sub-micron particles, such as gold nanoparticles,[1] quantum dots,[2] and magnetic particles[3–8] into superstructures, hosted in functional matrices, provides an avenue for producing multi-stimuli responsive materials. Liquid crystalline (LC) matrices are functional mediums that exhibit a plethora of ordering motives connected with directional and translational sensitivity to external stimuli. In recent experimental reviews[9,10] and approaches[3,5,11] is shown that LC matrices can be used for inducing the self organization of superstructures and nanoparticles.

Correspondingly, creating suspensions of magnetic nanoparticles (MNP) in liquid crystalline (LC) matrices, *i.e.* LC–MNP hybrid systems,[3,5,10] is a non-trivial strategy for obtaining materials that are sensitive both to external magnetic and electric fields. The simplest of LC–MNP hybrid, a ferronematic, was coined by Brochard and de Gennes[12] four decades ago; formulating the free energy in a mesoscopic model of colloidal MNP and thermotropic LCs, they have predicted that the system can be locally ferromagnetic without exhibiting macroscopic magnetization. Systematic efforts to synthesize ferronematics have produced a variety of colloidal suspensions of MNP in thermotropic low molar mass LCs.[13–15] Nevertheless, realization of a LC–MNP hybrid that consist of local ferromagnetic domains announced[3] two years ago. Early experiments in lyotropics have shown that lyomesophases doped with magnetic particles significantly alter the sensitivity of these systems to magnetic field[16,17] in comparison to undoped lyomesophases. There is also strong current interest[18] in lyotropic suspensions of colloidal rodlike LC and MNP spheres in which both species have comparable size. Further, experimental research has produced[19,20] colloidal suspensions of spherical magnetic particles with pigment rodlike particles.[21] These systems are quite promising regarding their sensitivity both to magnetic and electric fields, since even the mono-dispersed system of pigment rods exhibits non-conventional behavior (*e.g.* reversible phase separation upon application of an external electric field[21]).

Herein, we attempt to clarify the role of basic geometrical features of liquid crystalline and magnetic particles on the self-organization of such systems using molecular dynamics simulations. To this end we consider a rod-sphere mixture (see ref. 22 and 23) in which the magnetic particles are represented as soft dipolar spheres with an embedded dipole. We focus on situations where the length scales of the two species are comparable. Thus, our model is not appropriate for situations where the magnetic particles are much larger than the LC molecules (such as in ref. 3) and thus, induce strong distortions (for corresponding theoretical approaches, see ref. 12 and 24). Still, our model provides a realistic description of other experimental systems. For example, we have recently used our model to interpret the response of a real system[20]-consisting of LC pigment nanorods (of typical width of 40 nm) and magnetic spheres (of diameter 10 nm)-under an external magnetic field.

Institute of Theoretical Physics, Technical University Berlin, Secr. EW 7-1 Hardenbergstr. 36, D-10623 Berlin, Germany. E-mail: peroukid@mailbox.tu-berlin.de; Fax: + 49 30 314-21130; Tel: +49 30 314-28851

† Electronic supplementary information (ESI) available. See DOI: 10.1039/c6sm01264g

The constituent parts of this model (*i.e.* rod-sphere mixtures and monodispersed dipolar spheres) have already been studied extensively as it is shown below.

Nonmagnetic rod-sphere mixture systems have attracted considerable scientific interest. In particular, the phase behavior of such systems has been investigated by experiments,[25,26] theoretical studies[27–30] and computer simulations[31–34] revealing a rich polymorphism that includes re-entrance phase transitions as well as multiphase equilibria between isotropic, nematic, smectic and columnar phases. Our intention here is concentrated in fully miscible binary rod-sphere mixtures in various LC states.

Mono-dispersed dipolar sphere systems have also been studied intensively since it constitutes the simplest model of magnetic fluids (ferrofluids). Insight into the phase behavior of such systems has been obtained by analytical theories[35–39] and computer simulations.[35,39,40–46] These systems exhibit a variety of self-assembled micro-structures in which the dipolar spheres are arranged into head-to-tail configurations. In particular, they form ferromagnetic chains,[40–45] networks,[40,41,46] rings[40,43–45] and branched[43–45] structures. The stability of these structures has been related to thermodynamic variables of concentration and temperature. Experimental observations of magnetic particle assemblies in isotropic solutions can be found in ref. 6–8. Furthermore, the self-organization and assembly of the magnetic particles can be tuned by external fields giving rise to (infinite or finite) ferromagnetic chains in homogeneous magnetic fields,[47] formation of synchronized ferromagnetic layers in rotational fields,[48] cave structures in triaxial fields[49] with potential applications in biomedicine[50,51] and magneto-rheology.[52] Even though, an enormous effort has been devoted in mono-dispersed dipolar sphere systems, as it is shown above, there are a few simulation studies[22,23] that take into account explicitly the presence of an anisotropic medium (*e.g.* a LC matrix) in dipolar spheres suspensions. In this paper we attempt to further contribute to this scientific research.

This work has a two-fold purpose: firstly, to examine under what conditions the magnetic particles self assembly into superstructures in LC matrices and, more importantly, how the anisotropic medium promotes the self-organization of these assemblies. Secondly, by monitoring the evolution of the system with time we examine the translational dynamics both in the isotropic state and LC matrices. To the best of our knowledge, the study both of structure and dynamics of magnetic particle assemblies (clusters) in LC matrices using simulations is missing from the research literature. In earlier Monte Carlo simulations[22,23] we have focused on systems in which the diameter of spheres is equal or greater than the width of the rods; consequently, the magnetic particles form infinite or fragmented chains that organize into uniaxial and biaxial states. In the present work, we scrutinise the opposite direction, by studying both the structure and dynamics in mixtures of rods and relative small magnetic spheres (*i.e.* of diameter smaller than the width of the rods). In other words, we give emphasis to both static and dynamic properties of such systems. This is challenging, both from theoretical and the ongoing experimental perspective, since this model system is closer to the real suspensions of rod-magnetic sphere particles.[19,20]

The model and simulation details are presented in Section 2. Our results for the ordering and structure of the magnetic particles assemblies in the LC matrices are presented and discussed in Section 3.1. In Section 3.2 we present the evolution of the system with time and the corresponding translational dynamic mechanisms. Finally, the conclusions are presented in Section 4.

2 Model and simulations details

We have studied binary mixtures of N_r Gay Berne (GB) rods and N_s dipolar soft spheres (DSS), with an embedded permanent point dipolar moment μ in their center. Here we provide a brief description of the parametrization of the model that is used; a more detailed presentation is given elsewhere.[22,23] The rods interact *via* an anisotropic (orientational dependent) attractive–repulsive GB potential.[32] The GB potential is of Lennard-Jones form incorporating an orientation dependent range; it depends both on the orientation and interparticle distance of two anisotropic particles. We have set the length (l) to width (σ_0) aspect ratio $l/\sigma_0 = 3$. We have chosen this value since (i) corresponds to a well studied mono-dispersed GB system,[53] and (ii) it is in the accessible limit, though in the lowest, of experimentally investigated real rodlike liquid crystalline colloidal suspensions.[19,20] The DSS particles interact *via* a soft repulsive potential and a dipole–dipole interaction.[22,23] The diameter of the DSS particles is set $\sigma_s^* = \sigma_s/\sigma_0 = 0.25$ (*i.e.* it is four times smaller than the width of the rods comparable with that in corresponding experimental systems[19,20]). A systematic examination of mixtures with spheres diameter equal or greater than the width of the rods has been reported elsewhere.[22,23] The long range interactions are handled by the implementation of the three dimensional Ewald sum.[54] The reduced permanent point dipole moment is set to $\mu^* = \mu \Big/ \sqrt{\varepsilon_0 \sigma_s^3} = 3$ (or 3.5 in some cases), and the reduced temperature is $T^* = k_B T/\varepsilon_0$ (with k_B being Boltzmann's constant and ε_0 is energy parameter of the GB interaction[23]). The dipolar coupling parameter $\lambda = \mu^2/kT\sigma_s^3$ then takes values greater than 6, which is characteristic of strongly coupled magnetic particles.[46,55,56] Finally, for interaction of rods and spheres we consider a modified GB potential.[32,57] The modified GB potential depends only on the orientation of the rods and the interparticle distance vector of the center of mass of rods and spheres.

We have implemented extensive molecular dynamics (MD) simulations[58] using $N = N_s + N_r$ particles at constant volume V and (kinetic) temperature T. We have used the leap-frog algorithm[58,59] to handle the equations of motion. We have examined binary mixtures of GB–DSS particles for a fixed particle composition $x_r = N_r/N = 0.8$ and volume fraction ratio $\phi_r/\phi_s = 780$ (where $\phi_a = N_a u_a/V$ is the volume fraction and u_a is the volume of particle a = r, s-for rods and spheres, respectively-) and for various number densities $\rho^* = N\sigma_0^3/V$. The volume fraction ratio, ϕ_r/ϕ_s, is quite high in comparison to previous

studies[22,23] in which the corresponding value is one or two orders of magnitude smaller. An important advantage of studying suspensions of magnetic particles of relative high volume fraction ratio, ϕ_r/ϕ_s, is that this permits to examine the influence of the LC matrix on the magnetic particle assemblies rather than the other way round. The reduced moment of inertia is set for both particles to $I^* = I/m\sigma_0^2 = 1.0$ and a time step $\Delta t^* = 0.002$ (where the reduced time $t^* = \sqrt{\varepsilon_0/m\sigma_0^2}t$). Equilibration requires a length of a least 10^6 time steps and further 10^6 time steps are used for producing ensemble average.

3 Results and discussion

3.1 Self organization of magnetic particles assemblies

We have examined GB–DSS mixtures consisting of $N = 2000$ or 4000 particles for composition $x_r = 0.8$; the systems show statistically equivalent results. We have performed cooling series using as initial configuration either an isotropic phase or a nematic phase (obtained by melting a crystal state) with a homogeneous distribution of the DSS particles in the simulation box. The reversibility of the states has been tested for selected state points $[(T^*, \rho^*)]$ by performing heating series from positionally ordered states. The state diagram in a $[(T^*, \rho^*)]$ presentation is shown in Fig. 1. Here, we have set $\mu^* = 3.0$. We should note that this diagram shows states in equilibrium. Our intention here is not to locate the phase transition boundaries. The calculation of the exact phase boundaries requires simulation techniques and methods to calculate the absolute free energy (see for example ref. 60) that exceed the scope of this paper. Optical observations indicate that only one phase is present in the simulation box of each state point. In that sense we provide an overview of the phases exhibited. The states are indicated in the diagram by different symbols. We have obtained three fully miscible phases (categorised with respect to the ordering of the GB particles), namely: (i) an isotropic (I), a uniaxial nematic (N_u) and a smectic-B (SmB) phase. The topology of the diagram is similar to that of a pure GB system.[53] The dotted lines indicate, approximately, coexistence densities ($\rho^* = \rho_r^* N/N_r$) of pure GB system (the data for $\rho_r^* = N_r\sigma_0^3/V$ where taken from ref. 53). Note that the lines drawn a guide to the eye. Thus, the DSS particles do not exert strong perturbation on the LC matrix. As we have already mentioned, this is expected due to the small total volume of DSS in comparison to corresponding volume of the GB particles. In the I phase, the orientational order of GB species has been confirmed by the calculated global nematic order parameter $S^{(r)}$ that takes values essentially zero. The global nematic order parameter $S^{(a)}$ (with a = r, s) is calculated by diagonalization of the ordering matrix and extracting the largest eigenvalues[61] (see also ESI,† Section I). The N_u phase is a uniaxial phase similar to the pure GB system. At lower temperature the GB particles are arranged into layers forming a smectic phase that in addition exhibits hexagonal (in-layer) order indicative of a SmB phase. Depending on the coupling strength λ the DSS particles self-assemble into (finite) clusters as it is illustrated in Fig. 2. In the next subsections, we turn to understand the structure of the clusters of the magnetic particles and

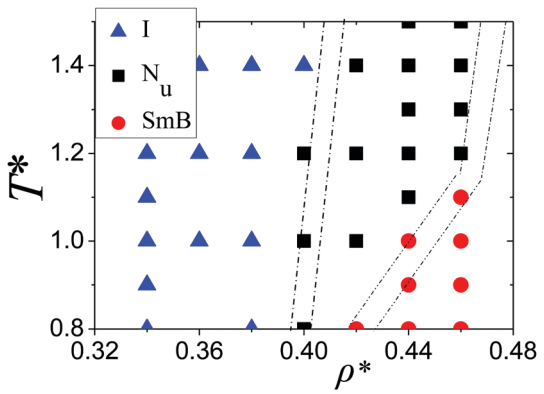

Fig. 1 (a) Tentative state diagram of a GB–DSS mixture with $\sigma_s^* = 0.25$ and $x_r = 0.8$. The points on the diagram indicate the pairs (T^*, ρ^*) for which the actual simulations were performed. The dipole moment is set $\mu^* = 3.0$. The dotted lines indicate, approximately, coexistence densities of the pure GB system.[53] Abbreviations: fully miscible isotropic (I), uniaxial nematic (N_u), uniaxial smectic (SmB) states.

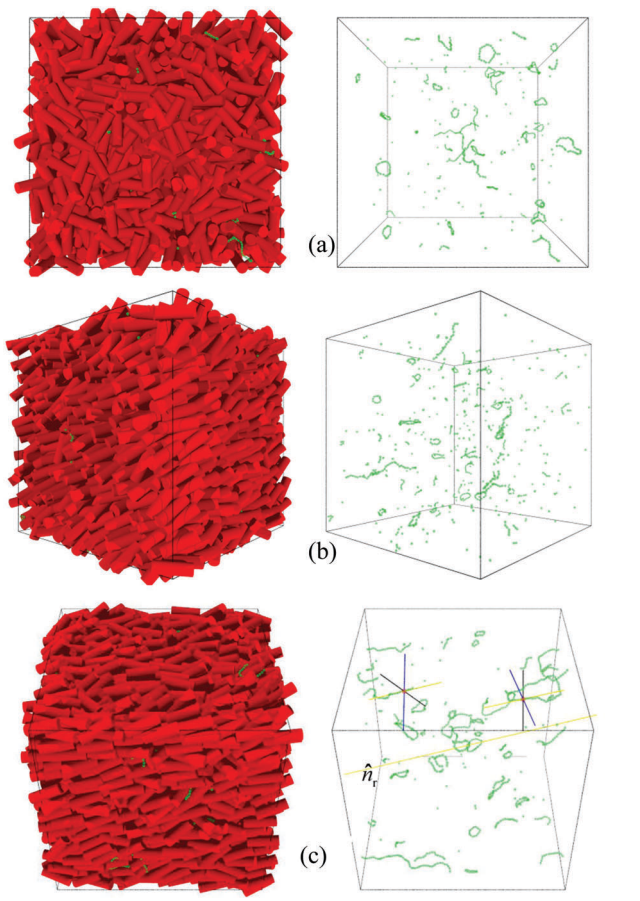

Fig. 2 Representative snapshots of a GB–DSS mixture with $\sigma_s^* = 0.25$ and $x_r = 0.8$ in various states: (a) isotropic state at $[(T^*, \rho^*) = (1.2, 0.34)]$, (b) uniaxial nematic ($N_u$) state at $[(T^*, \rho^*) = (1.4, 0.44)]$ and (c) uniaxial nematic (N_u) at $[(T^*, \rho^*) = (1.2, 0.44)]$. The direction of $\hat{\mathbf{n}}_r$ and the principal axis frames of a ring and a chain are also shown. For clarity, the rod species have been removed from the simulation box (right column).

the mechanisms that determine the organization of these structures in the LC matrix.

3.1.1 Clustering of magnetic particles. From the snapshots that are shown in Fig. 2 one clearly recognizes the presence of clusters of DSS particles in the LC matrix. The self assembly of DSS particles into clusters has been quantified by implementing the following procedure: We know the positions of the DSS particles at each time step (note that we obtain ensemble averages by collecting samples every 5000 time steps), (1) we begin with the DSS particle i, (2) secondly, a simple criterion is used to define a 'bond' between two particles. Specifically, two DSS particles i and j are considered bonded if their interparticle distance (r_{ij}) fulfils: $r_{ij} < r_{cl}$, where r_{cl} is set to $1.24\sigma_s$. (3) Another DSS particle l is 'bonded' with i if $r_{il} < r_{cl}$; moreover, if (i,j) are bonded then l is a member of the cluster (i,j,l) when either $r_{il} < r_{cl}$ or $r_{jl} < r_{cl}$. This process is continued to determine all DSS particles that form a cluster with DSS particle i. (4) We then continue the search of other clusters implementing the same process (1 to 3). The value of r_{cl} lies between the first maximum and minimum of the pair correlation function $g(r)$ and does not change considerably for the ρ^* and T^* we have examined (see ESI,† Section II, for representative $g(r)$). This minimal criterion, that is used here and based on geometrical considerations, simplifies the parameterization criterion relative to the one introduced in previous studies[45] that, in addition, uses a negative inter-particle energy fulfilment ($u(i,j) < 0$). After employing the above procedure to determine the clusters, we further categorize them according to their topology into: (i) chain clusters consisting of at least three particles (for which two particles of the cluster have one bond-*i.e.* the ends of the chain-), (ii) ring clusters (for which all particles of the cluster have two bonds), (iii) branched clusters (for which at least one particle of the cluster has three or more bonds) and (iv) "free" (non-bonded) particles and pairs of DSS particles. Therefore, the ring clusters and branched structures consist of at least three and four DSS particles, respectively. This is not surprising since small rings of three particles have also been observed in other theoretical studies.[45]

We have examined the size distribution of clusters for various state points [(T^*, ρ^*)] in the I, N_u and SmB phases. Initially, we investigate the self-assembly of particles into clusters for fixed $\rho^* = 0.44$ by varying the temperature T^* within the N_u and SmB phases. The calculated fractions of DSS particles into (i) rings, (ii) chains, (iii) branched structures, and (iv) "free" or pairs of particles as a function of temperature are presented in Fig. 3. As it is shown in the diagram, the majority of the particles form clusters of rings, chains, pairs or remain in the sample as "free" particles; whereas branched structures correspond only to a small fraction (lower than 0.1) that decays to 0.07 by decreasing the temperature to $T^* = 1.2$. On cooling, the fraction of the rings increases considerably from 0.1 (at $T^* = 1.4$) to 0.7 (at $T^* = 1.0$). At the same time the fraction of "free" and pairs of DSS particles decreases dramatically. The formation of chains has a peculiar behavior: it slightly increases from high to lower temperatures and then decreases. This behavior can be interpreted by the fact that the

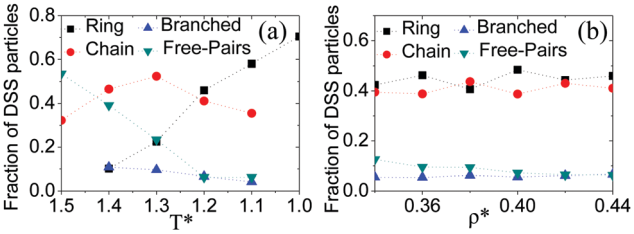

Fig. 3 (a) Fraction of DSS particles into various clusters dependence on temperature T^* along an isochore $\rho^* = 0.44$ and (b) fraction of DSS particles into various clusters dependence on density ρ^* along an isotherm $T^* = 1.2$. Different symbols are used to indicate: rings (square), chains (circles), branched structures (triangles) and 'free' or pairs (down triangles) clusters.

formation of rings become energetically more favourable at lower temperatures (*i.e.* by increasing the dipolar coupling λ). Rovigatti *et al.*[44,45] have found that in mono-dispersed dipolar hard spheres the fraction of ring clusters increases by lowering the temperature whereas chain clusters show the reverse behavior. Our results indicate that even in an anisotropic medium the DSS component exhibits qualitative similar behavior regarding the formation of chains and rings. In summary, we have found that the LC matrix does not prevent the formation of clusters. Rather the attractive–repulsive interaction between the GB and DSS particles supports the formation of clusters.

The clusters size distribution $n(k)$ (with k being the number of particles in the cluster) of all types along an isochore $\rho^* = 0.44$ and various temperatures is presented in Fig. 4a. Lowering the temperature promotes the formation of larger clusters; consequently, the amount of clusters consisting of few particles decreases. Furthermore, for $T^* \leq 1.4$ we observe a local maximum of $k \approx 10 - 20$ that is related to the contribution from ring clusters. This is proven both by an increment of the fraction of the rings in the sample (see Fig. 3) and by the diagram of the distribution $n_r(k)$ of the ring clusters that is shown in Fig. 4b. It is evident that $n_r(k)$ exhibits a maximum for size $k \approx 10$ and shows a tail at lower temperatures indicating the presence of even larger clusters. The cluster distribution of the chains $n_c(k)$ does not show any local maxima and decays as the cluster size k is increased (see Fig. 4c). At lower temperatures the tail of the distribution expands to larger cluster size k indicating an increment of the mean size of the chains.

We now turn to study the clusters distribution dependence on the density ρ^* at constant temperature $T^* = 1.2$. As it can be seen from Fig. 4d–f the behavior is qualitatively similar for the whole range of densities examined. This is also reflected in the populations of clusters that do not change significantly with density (see Fig. 3b). This demonstration is a non-trivial finding with consequences yet to be explored in the design of real suspensions (*e.g.* in ref. 20) of magnetic particles in LC matrices. The fact that the orientational state of the matrix (isotropic *versus* nematic) does not significantly change the cluster types and their size distributions suggests, on the one hand, that the (free) energy landscape determining the cluster formation is similar to the case of pure DSS particles (without the matrix).

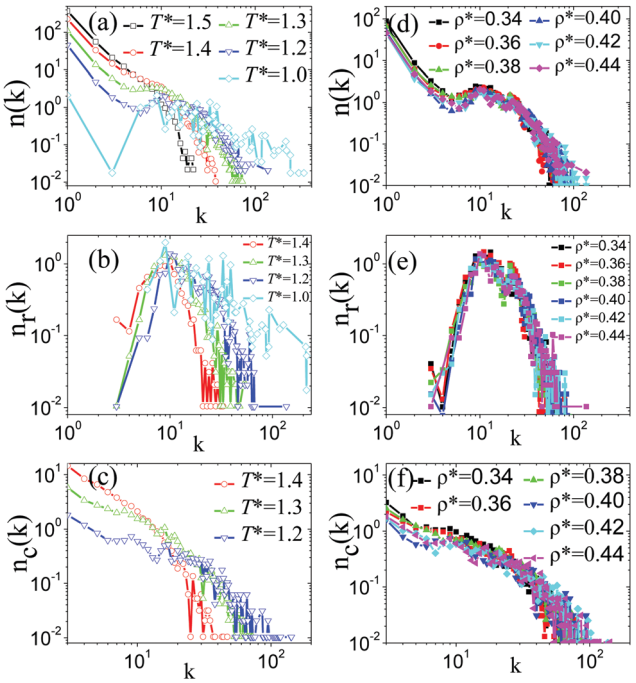

Fig. 4 (a–c) Number of clusters of arbitrary type $n(k)$, rings $n_r(k)$ and chains $n_c(k)$ of size k for several temperatures T^* along an isochore $\rho^* = 0.44$. (d–f) Number of clusters $n(k)$, rings $n_r(k)$ and chains $n_c(k)$ of size k for several densities ρ^* along an isotherm $T^* = 1.2$.

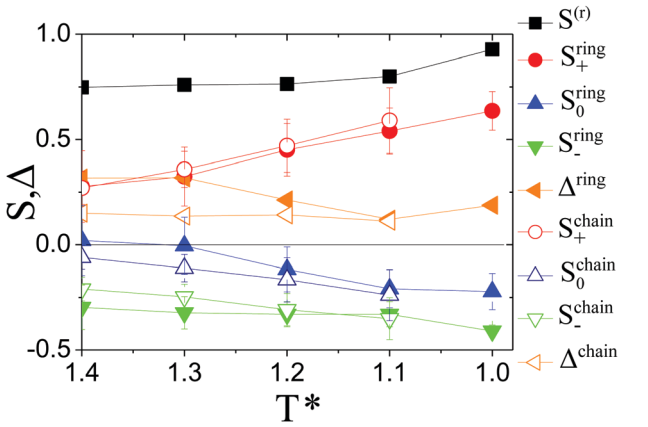

Fig. 5 Order parameters of clusters S_b^{cl} dependence on temperature T^* for constant $\rho^* = 0.44$ and $\mu^* = 3.0$. Solid symbols correspond to the global order parameter of the rods and ring clusters; open symbols correspond to chain clusters.

This might be a consequence of the fact that the particles are too small to feel the character of the matrix. On the other hand, our results reveal that the matrix in its nematic state induces an average orientational ordering of the clusters (see Section 3.1.2), showing that the cluster structures (and thus the landscape) does respond, to some extent, to the matrix.

3.1.2 Orientational ordering of clusters in the LC matrix. In this subsection we examine the orientational ordering of clusters as individual entities in the LC matrix. Indeed, the global order parameter $S^{(s)}$ of the DSS particles can not measure the orientational order of the clusters in the LC matrix. Below, we describe the method we have used[20] to monitor the orientational order of the clusters (see also ESI,† Section I): (i) initially, we calculate the nematic director ($\hat{\mathbf{n}}_r$) for the entire system, (ii) secondly, we construct the ordering matrix of each cluster and from the extracted eigenvalues $S_+^{cl} > S_0^{cl} > S_-^{cl}$ we get the corresponding eigenvectors $\hat{\mathbf{n}}_+^{cl}$, $\hat{\mathbf{n}}_0^{cl}$ and $\hat{\mathbf{n}}_-^{cl}$ (this set of eigenvectors defines a local principal axis frame for each cluster), and (iii) finally, we calculate ensemble averages of the clusters order parameters that are given by $S_b^{cl} = \langle P_2(\hat{\mathbf{n}}_r \cdot \hat{\mathbf{n}}_b^{cl})\rangle$, with $b = +, -, 0$ and P_2 the second legendre polynomial. The order parameter S_b^{cl} shows the orientational order of the local principal axis of the cluster with respect to the director $\hat{\mathbf{n}}_r$ of the whole system. Here, 'cl = ring or chain' for rings and chains, respectively. The $\hat{\mathbf{n}}_+^{cl}$ is the major axis of the cluster (either ring-of elliptical shape-or of 'snake-like' chains). The other two eigenvalues are perpendicular to $\hat{\mathbf{n}}_+^{cl}$. For example, in a uniaxial linear chain, S_0^{cl} is equal to S_-^{cl} and therefore the corresponding eigenvectors can be any vector that is perpendicular to $\hat{\mathbf{n}}_+^{cl}$.

A plot of the S_b^{cl} order parameters at various temperatures in the N_u and SmB phase for $\rho^* = 0.44$ is given in Fig. 5. Interestingly, the S_+^{cl} order parameter has relatively large positive value -between 0.4 and 0.6 both for rings and chains-whereas the other two are not equal and have negative (or near to zero) values. This clearly indicates that the major axes $\hat{\mathbf{n}}_+^{cl}$ of the clusters tend to be, on average, parallel to $\hat{\mathbf{n}}_r$. We conclude that the LC matrix induces orientational order to the clusters. An illustration of the local principal axis frame of a ring and a chain is shown in Fig. 2c. This type of alignment is not found in the isotropic phase in which the S_b^{cl} parameters are close to zero. Calculations of corresponding pure dilute dipolar systems (by dropping the LC particles and keeping the same volume) show that there is no orientational order in these systems. The same behavior is expected in pure, relative dilute, isotropic systems of dipolar spheres reported in ref. 45. The alignment of the clusters is enhanced at lower temperatures in which more 'tight' clusters are formed. The non-uniaxiality of the shape of the clusters is shown by the inequality of the other two values S_0^{cl} and S_-^{cl} (see Fig. 5). Indeed, the nonvanishing $\Delta = S_0^{cl} - S_-^{cl}$ shows deviation from a uniaxial shape (*i.e.* either of linear-chains or circle-rings) that is more pronounced in the case of ring clusters (see Fig. 5). In the nematic states the order parameter of rings Δ^{rings} is greater than the order parameter of chains Δ^{chains}. Furthermore, one of the principal axes of the ring clusters $\hat{\mathbf{n}}_0^{cl}$ tends to be perpendicular to $\hat{\mathbf{n}}_r$ with the corresponding order parameter of rings being $-0.25 \leq S_0^{cl} \leq 0$. The remaining axis, $\hat{\mathbf{n}}_-^{cl}$, follows the motion of $\hat{\mathbf{n}}_+^{cl}$ and $\hat{\mathbf{n}}_0^{cl}$ since they form an orthogonal frame. Hence, even though the LC matrix posses uniaxial symmetry, the clusters do not rotate freely around the axis of alignment (*i.e.* $\hat{\mathbf{n}}_+^{cl}$) due to their non-uniaxial shape.

In the next subsection we keep the matrix at the same conditions (nematic) and examine the impact of a stronger dipole moment μ^* on the cluster formation and their orientational order.

3.1.3 Ordering and clusters size distribution for a stronger dipole moment of the magnetic particles. Let as now examine the clusters' size distribution in the nematic phase by considering

stronger dipole moment of the DSS at a fixed state point. Specifically, we have studied the case $\mu^* = 3.5$ (as compared to $\mu^* = 3.0$), yielding $\lambda = 10.2$ (as compared to $\lambda = 7.5$) at $[(T^*, \rho^*) = (1.2, 0.44)]$ in the N_u state. Over 98/100 of the particles participate in the formation of ring type clusters whereas all other types nearly extinguish. A snapshot that illustrates this is given in Fig. 6. This is another confirmation that strong dipolar interactions favour the formation of ring clusters. In practice, the total clusters distribution, $n(k)$, coincides with $n_r(k)$ and is presented in Fig. 6b. The $n(k)$ distribution becomes flat and does not show a maximum as in the case of smaller dipole moment *i.e.* $\mu^* = 3.0$. This means that rings of cluster size 10–100 coexist in the sample and are distributed homogeneously in the LC matrix (see Fig. 6a). These results show that there are both quantitative (regarding the type of distribution) and qualitative (regarding the type of dominant clusters) differences in comparison to a system of smaller μ^*. Moreover, the orientational ordering of the clusters in the N_u phase is clearly enhanced with S_+^{ring} increment from 0.45 ($\mu^* = 3.0$) to 0.60 ($\mu^* = 3.5$). The order parameter $\Delta = S_0^{ring} - S_-^{ring} \approx 0.19$ is essentially equal to the system with smaller μ^*. Note also that the corresponding order of the N_u phase is not affected indicating that the presence of clusters does not exert strong perturbation in the LC matrix properties.

3.2 Translational dynamics of magnetic particles in the LC matrix

In this section we investigate the diffusion properties of the DSS particles in the LC matrix. The translational dynamics have been investigated by the evaluation of the mean-square displacement (MSD):[62]

$$\left\langle |\Delta \mathbf{r}(t)|^2 \right\rangle = \frac{1}{N_s} \sum_{i=1}^{N_s} \left\langle |\mathbf{r}_i(t) - \mathbf{r}_i(0)|^2 \right\rangle \quad (1)$$

For a typical fluid, the MSD function is for short times proportional to t^2 indicating a short time ballistic regime, followed by a diffusion regime where $\langle |\Delta \mathbf{r}(t)|^2 \rangle \sim t$. Through Einstein's relation[62] at sufficiently long times we can calculate the self diffusion coefficient of the DSS particles,

$$D = \lim_{t \to \infty} \frac{\left\langle |\Delta \mathbf{r}(t)|^2 \right\rangle}{6t} \quad (2)$$

In an orientationally ordered LC matrix (*e.g.* in the N_u or SmB state) it is expected that the diffusion coefficients parallel ($D_\parallel$) and perpendicular ($D_\perp$) to the director $\hat{\mathbf{n}}_r$ are different. These diffusion coefficients are related through[63] $6D = 2D_\parallel + 4D_\perp$. The MSD as a function of reduced time is given in Fig. 7a for several temperatures, along the isochore $\rho^* = 0.44$. At high temperature ($T^* = 1.4$), in the N_u state, the MSD is proportional to t^2 (ballistic regime) and approach the linear "Einstein's" regime at longer times. At lower temperature ($T^* = 1.2$), still in the N_u state, a sub-diffusive regime appears (for time range $(0.1 < t^* < 1)$). At even lower temperature ($T^* = 1.0$), in the SmB state, the normal diffusive regime is barely reached within long time simulation runs of over 10^6 time steps. Nevertheless, the fact that we do reach the diffusive regime suggests normal, fluid-like (rather than glass-like) behaviour. For states of $T^* > 1.0$ the linear diffusive regime is reached at less than 10^5 time steps (see Fig. 7a). In the ESI,† Section III we also present dipole–dipole autocorrelation functions that decay to zero within the simulation time runs, indicating a fluid behavior with respect to the magnetic particles orientations. Due to both the long range and local (hexagonal) translational ordering of the SmB state, the magnetic particles become dynamically arrested covering only short distances even at very long times.

The dependence of the total diffusion coefficient D on temperature derived from the slope of MSD, which is $6D$, (see eqn (2)) at long times (linear regime), is shown in Fig. 7c. The corresponding slopes provide $2D_\parallel$ and $4D_\perp$. A linear fit of the diffusion coefficients is also given in Fig. 7b. Clearly, the equation[63] $6D = 2D_\parallel + 4D_\perp$ is verified (see also Fig. 7c). As it can be seen D increases by temperature for a given dipole moment ($\mu^* = 3.0$). This has also been observed in pure systems of dipolar dumbbells using simulations.[64] This behavior can be rationalized as follows: the percentage of "free" DSS particles decreases by lowering the temperature giving place to the formation of clusters that slow down the mobility of DSS particles.

Further, we find that the diffusion of magnetic particles is different in parallel and perpendicular directions. An example of calculated MSD parallel $\langle |\Delta \mathbf{r}_{||}(t)|^2 \rangle$ and perpendicular $\langle |\Delta \mathbf{r}_\perp(t)|^2 \rangle$ to $\hat{\mathbf{n}}_r$ are shown in Fig. 7b. The difference of the coefficients is indicated by the diffusion anisotropy $A = (D_{||} - D_\perp)/D$ that is shown in Fig. 7c. Further, A varies with T^* within the N_u state. This means that the formation of more strongly 'bonded' clusters,

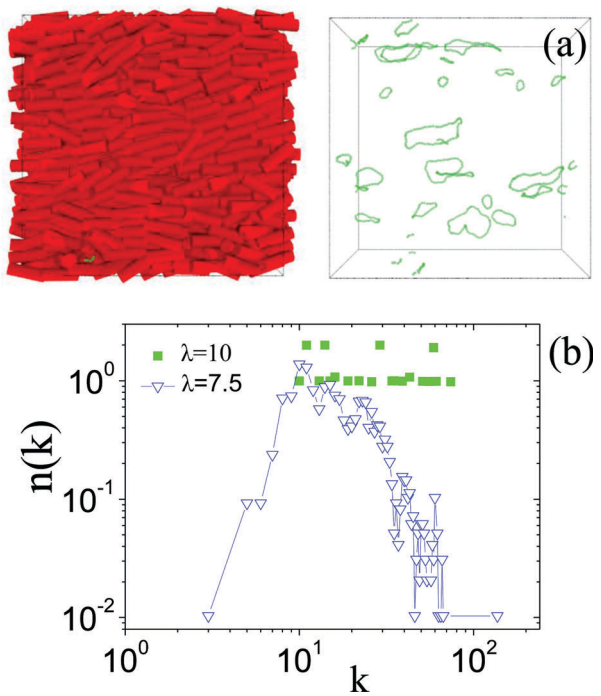

Fig. 6 (a) Representative snapshots at state point $[(T^*, \rho^*) = (1.2, 0.44)]$ in the N_u phase for $\mu^* = 3.5$. It is evident that ring clusters are dominant and (b) ring type clusters $n_r(k)$ size distribution for $\mu^* = 3.5$ (squares) and $\mu^* = 3.0$ (down triangles).

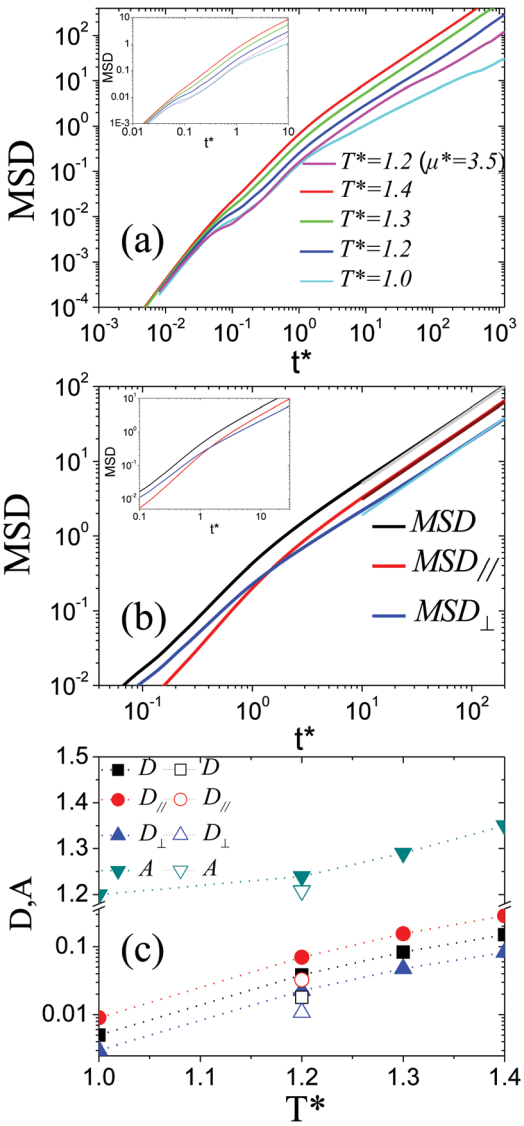

Fig. 7 (a) Total mean square displacement (MSD) for fixed dipole moment $\mu^* = 3.0$ (exceptions are indicated), (b) direction resolved MSD parallel and perpendicular to the nematic director in N_u state at [(T^*, ρ^*) = (1.3, 0.44)] (linear fits MSD-grey-, MSD parallel-dark red and MSD perpendicular-cyan-) and (c) diffusion coefficients D, parallel $D_{\parallel}$, perpendicular $D_{\perp}$ to the nematic director, and diffusion anisotropy parameter A. Close and open symbols correspond to dipolar moment $\mu^* = 3.0$ and $\mu^* = 3.5$, respectively. The results were taken for various temperatures T^* along an isochore $\rho^* = 0.44$.

occurring at lower temperatures due to an increase of λ, leads to smaller A. Interestingly, at short times the magnetic particles travel faster perpendicular to the nematic director. This behavior is reversed at longer times (linear diffusive regime) and the motion parallel to the LC director becomes faster. Therefore, the LC matrix induces orientational order to the clusters (see also Section 3.1.2) and promotes their long time collective motion along the director.

We have also calculated the MSD dependence on time t^* in Fig. 8a for several densities, along an isotherm ($T^* = 1.2$). The system reaches the diffusive 'linear regime' for all densities examined.

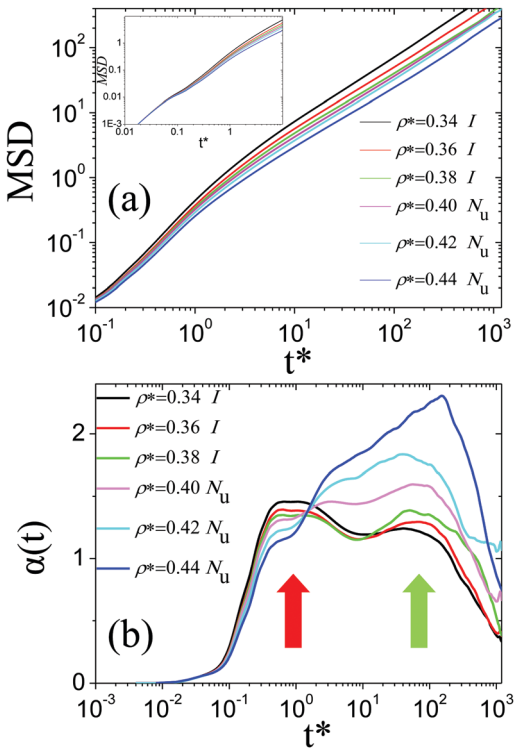

Fig. 8 (a) Mean square displacement (MSD) and (b) non-gaussian parameter $\alpha(t)$ dependence on time for several densities ρ^* along an isotherm $T^* = 1.2$. The dipole moment $\mu^* = 3.0$.

As it is expected at higher densities the reduced diffusion coefficient D (not shown here) decreases.

To further monitor the translational dynamics in our system we have calculated the 'non-gaussian' parameter[65]

$$\alpha(t) = \frac{3\left\langle |\Delta \mathbf{r}(t)|^4 \right\rangle}{5\left\langle |\Delta \mathbf{r}(t)|^2 \right\rangle^2} - 1 \qquad (3)$$

By definition, $\alpha(t)$ is zero in perfectly ballistic or perfectly diffusive regimes, deviations from zero thus indicate non-trivial behavior. As seen from Fig. 9 the $\alpha(t)$ is a non-monotonic for several temperatures and constant density $\rho^* = 0.44$. At high temperature ($T^* = 1.4$), in the N_u state, it initially increases and then decays smoothly as the system passes from the ballistic to the diffusive regime. This behavior is also evident by the MSD that is shown in Fig. 7a. Note that at this state point a large amount of particles do not form clusters (see Fig. 3). At intermediate temperature ($T^* = 1.2$) starting from the ballistic regime, $\alpha(t)$ exhibits various modes and rises ($t^* \approx 100$) before starting decreasing as the system passes to the linear regime. The sub-diffusive regime that is detected by the MSD function (see Fig. 7a) is indicated here by a plateau in the time range $0.1 < t^* < 1$ (see Fig. 9). This time period corresponds to translational motion of length scale $0.1\sigma_o$ to $1\sigma_o$ that is of the order of magnitude of the size of DSS particles or very small clusters. Therefore, it corresponds to intra-cluster correlations in a non-ballistic and non-diffusive regime. At even lower temperature ($T^* = 1.0$), in the SmB state, $\alpha(t)$ rises sharply and

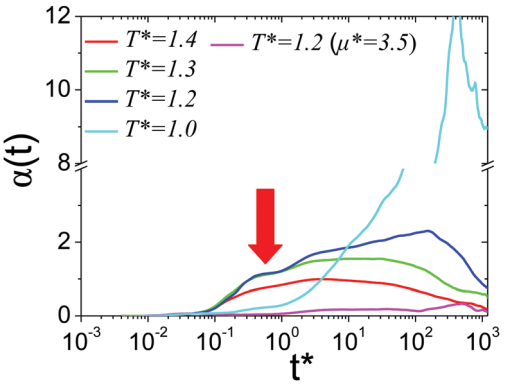

Fig. 9 Non-gaussian parameter $a(t)$ dependence on time for several temperatures T^* along an isochore $\rho^* = 0.44$ (with $\mu^* = 3.0$). It is also shown the corresponding quantities for a system with stronger dipolar moment (with $\mu^* = 3.5$).

decays for long times that correspond to diffusive regime (see Fig. 9). This is caused because the local and long range positional order of SmB "traps" various clusters, slowing down differently their motion within the sample. Therefore, the smectic structure significantly affects the collective motion of the magnetic particles. Non-gaussian dynamics has also been found[66] in pure hard rods systems in the smectic phase due to the layered structure and cooperative motion of rod particles within the phase. On the other hand, in a system of a relatively strong dipole moment, *i.e.* $\mu^* = 3.5$, in the same N_u state (see Section 3.1.3), the presence of dominant well defined rings suppresses this behavior. This is shown in Fig. 9 in which $a(t)$ takes relative small values. Nevertheless, the diffusion coefficients decrease in comparison to a system with smaller μ^* in the same N_u state (see Fig. 7c open symbols).

We now turn to examine the behavior of the system along an isotherm ($T^* = 1.2$). The $\alpha(t)$ parameter indicates that the dynamics of the system show qualitative difference as the system goes from the low to high densities at an isotherm ($T^* = 1.2$) (see Fig. 8b). Indeed, at low densities in the isotropic phase two plateau are found. The first one, indicated by a red arrow, corresponds to short times $t^* \approx 1$. As we have already mention this is related to intra-cluster correlations. The other plateau, is indicated by a green arrow, (reduced in height) is found at long times $t^* \approx 100$. At even longer times, by approaching the linear diffusive regime the $\alpha(t)$ decays to zero. At higher densities (in the N_u state) the second peak in the $\alpha(t)$ plot rises before the DDS particles reach the diffusive regime. This may be caused by the anisotropy of the LC matrix as it transforms from an isotropic to a nematic state. A similar interpretation was given above regarding the behavior of $\alpha(t)$ in the SmB state. The non-monotonic behavior of $a(t)$ indicates that the assembly and disassembly of clusters (chains, rings and branched structures) can be attributed to two modes: one corresponding to short times (intra-clusters correlations-first plateau-) and another corresponding to longer times (inter-cluster correlations-second plateau-).

4 Conclusions

In this work, using extensive molecular dynamics simulations we have studied the orientational and dynamical behavior of magnetic particles in liquid crystal matrices. We have implemented a simple model system comprising of Gay–Berne rods and dipolar soft spheres in which their diameter is smaller than the width of the rods. This prototype properly matches for addressing fundamental problems regarding the organization of magnetic particles in liquid crystalline ferrofluids.

We have observed the presence of magnetic particle assemblies (clusters) within the LC matrices. The matrix either in isotropic or in the LC state does not prevent the assembly of the magnetic particles into clusters. Hence, the host supports these structures. Nevertheless, their type as well as the quantity of DSS particles that form clusters depends crucially on the dipolar coupling strength between DSS particles. Two main types of clusters are exhibited, namely, rings (closed loops) and chains in which the DSS particles self-assembly into head-to-tail configuration. Interestingly, a small amount of branched structures is found indicating that their stability is not favoured in the binary mixtures we have examined. The anisotropic matrix (either in the nematic or in the SmB state) promotes the orientational order of the clusters indicating that it can be used as a template for the self-organization of magnetic particle assemblies. Tuning the dipolar strength, within the same nematic state, causes qualitative and quantitative changes on the properties of clusters. In particular, by rising the dipolar strength, ring clusters become dominant and their orientational ordering increases. The ordering of the nematic host does not change due to small perturbation that is exerted from the magnetic particles. This is in contrast to liquid crystalline magnetic particles systems[22,23] in which the volume fraction of magnetic particles is comparable to the LC particles and the orientational ordering of the matrix is influenced. Suitable orientational order parameters suggest that the clusters posses a non-uniaxial shape ("snake"-like chains and ellipsoidal rings).

Furthermore, we have analysed the dynamical behavior of the DSS particles in the LC matrix. At a moderate dipolar coupling strength, in which a relative small number of clusters is formed, the DSS particles go smoothly from the ballistic to the linear diffusive regime. A sub-diffusive regime appears for stronger dipolar strength between the ballistic and linear diffusive regime. An anisotropy in diffusivity of the magnetic particles in space occurs that is induced by the LC matrix. It is found that the diffusion constant parallel is greater than the diffusion constant perpendicular to the nematic director. At long times the magnetic particles travel faster along the director of the phase, whereas, at short times the reversed behavior is found. The non-gaussian parameter indicates the presence of different collective motion of various clusters in the sample that depend on the orientational and translational ordering of the matrix. Therefore, we have found that both the LC state of the matrix and the dipolar coupling strength plays an important role on the translational dynamics of the DSS particles.

Our findings provide a coherent frame under which the structure and dynamical properties of complex LC ferrofluids can be understood. This frame constitutes an exemplary tool that can be used to gain physical insight into and interpret the behaviour of experimental systems. Current research[20] shows that magnetic field induced structural transformations in such systems, by varying the strength of the field and the composition of the magnetic particles, opens up a route for the design of new functional materials with potential application as LC/MNP hybrid displays. An other interesting point that is also under examination[67] is who light propagation is influenced by morphological transformations of the magnetic particles within the matrix. Therefore, our results are of interdisciplinary character and may combine theoretical, simulations and experimental fields of fundamental research.

Acknowledgements

Financial support from the German Science Foundation (DFG) *via* the priority programme SPP 1681 is gratefully acknowledged.

References

1 Q. Liu, M. G. Campbell, J. S. Evans and I. I. Smalyukh, *Adv. Mater.*, 2014, **26**, 7178–7184.
2 M. F. Prodanov, N. V. Pogorelova, A. P. Kryshtal, A. S. Klymchenko, Y. Mely, V. P. Semynozhenko, A. I. Krivoshey, Y. A. Reznikov, S. N. Yarmolenko, J. W. Goodby and V. V. Vashchenko, *Langmuir*, 2013, **29**, 9301–9304.
3 A. Mertelj, D. Lisjak, M. Drofenik and M. Čopič, *Nature*, 2013, **504**, 237.
4 G. Ferk, P. Krajnc, A. Hamler, A. Mertelj, F. Cebollada, M. Drofenik and D. Lisjak, *Sci. Rep.*, 2015, **5**, 11395.
5 B. Matt, M. K. Pondman, B. Asshoff, J. S. ten Haken, B. Fleury and N. Katsonis, *Angew. Chem., Int. Ed.*, 2014, **35**, 12446–12450.
6 A. Wei, S. V. Pusztay, S. L. Tripp and R. Balasubramanian, *J. Inclusion Phenom. Macrocyclic Chem.*, 2001, **41**, 83.
7 S. L. Tripp, S. V. Pusztay, A. E. Ribbe and A. Wei, *J. Am. Chem. Soc.*, 2002, **124**, 7914.
8 S. L. Tripp, R. E. Dunin-Borkowski and A. Wei, *Angew. Chem., Int. Ed.*, 2003, **42**, 5591–5593.
9 C. Blanc, D. Coursault and E. Lacaze, *Liq. Cryst. Rev.*, 2013, **1**, 83–109.
10 S. Saliba, C. Mingotaud, M. L. Kahn and J.-D. Marty, *Nanoscale*, 2013, **5**, 6641.
11 J. Milette, S. Relaix, C. Lavigne, V. Toader, S. J. Cowling, I. M. Saez, R. B. Lennox, J. W. Goodby and L. Reven, *Soft Matter*, 2012, **8**, 6593–6598.
12 P. de Gennes and F. Brochard, *J. Phys.*, 1970, **31**, 691–708.
13 S.-H. Chen and N. M. Amer, *Phys. Rev. Lett.*, 1983, **51**, 2298–2301.
14 P. Kopčanský, N. Tomašovičová, M. Koneracká, V. Závišová, M. Timko, A. c. v. Džarová, A. S Šprincová, N. Éber, K. Fodor-Csorba, T. Tóth-Katona, A. Vajda and J. Jadzyn, *Phys. Rev. E: Stat., Nonlinear, Soft Matter Phys.*, 2008, **78**, 011702.
15 O. Buluy, S. Nepijko, V. Reshetnyak, E. Ouskova, V. Zadorozhnii, A. Leonhardt, M. Ritschel, G. Schonhense and Y. Reznikov, *Soft Matter*, 2011, **7**, 644–649.
16 L. Liebert and A. Martinet, *J. Phys. Lett.*, 1979, **40**, L–363.
17 A. Figueiredo Neto and M. Saba, *Phys. Rev. A: At., Mol., Opt. Phys.*, 1986, **34**, 3483.
18 S. Kredentser, O. Buluy, P. Davidson, I. Dozov, S. Malynych, V. Reshetnyak, K. Slyusarenko and Y. Reznikov, *Soft Matter*, 2013, **9**, 5061–5066.
19 Private communication with R. Stannarius group.
20 K. May, A. Eremin, R. Stannarius, S. D. Peroukidis, S. H. L. Klapp and S. Klein, *Langmuir*, 2016, **32**, 5085–5093.
21 K. May, R. Stannarius, S. Klein and A. Eremin, *Langmuir*, 2014, **30**, 7070–7076.
22 S. D. Peroukidis and S. H. L. Klapp, *Phys. Rev. E: Stat., Nonlinear, Soft Matter Phys.*, 2015, **92**, 010501(R).
23 S. D. Peroukidis, K. Lichtner and S. H. L. Klapp, *Soft Matter*, 2015, **11**, 5999–6008.
24 T. Araki and H. Tanaka, *Phys. Rev. Lett.*, 2006, **97**, 127801.
25 M. Adams, Z. Dogic, S. L. Keller and S. Fraden, *Nature*, 1998, **393**, 349–352.
26 N. Yasarawan and J. S. van Duijneveldt, *Soft Matter*, 2010, **6**, 353–362.
27 G. A. Vliegenthart and H. N. W. Lekkerkerker, *J. Chem. Phys.*, 1999, **111**, 4153–4157.
28 J. M. Brader, A. Esztermann and M. Schmidt, *Phys. Rev. E: Stat., Nonlinear, Soft Matter Phys.*, 2002, **66**, 031401.
29 S. D. Peroukidis, A. G. Vanakaras and D. J. Photinos, *J. Mater. Chem.*, 2010, **20**, 10495–10502.
30 G. Cinacchi, L. Mederos and E. Velasco, *J. Chem. Phys.*, 2004, **121**, 3854–3867.
31 P. G. Bolhuis, J. M. Brader and M. Schmidt, *J. Phys.: Condens. Matter*, 2003, **15**, S3421.
32 D. Antypov and D. J. Cleaver, *J. Chem. Phys.*, 2004, **120**, 10307–10316.
33 N. Urakami and M. Imai, *J. Chem. Phys.*, 2003, **119**, 2463–2470.
34 Z. Dogic, D. Frenkel and S. Fraden, *Phys. Rev. E: Stat., Nonlinear, Soft Matter Phys.*, 2000, **62**, 3925–3933.
35 G. N. Patey, D. Levesque and J. J. Weis, *Mol. Phys.*, 1979, **38**, 219.
36 M. A. Osipov, P. I. C. Teixeira and M. M. TelodaGama, *Phys. Rev. E: Stat., Nonlinear, Soft Matter Phys.*, 1996, **54**, 2597.
37 T. Tlusty and A. S. Safran, *Science*, 2000, **290**, 1328–1331.
38 S. Kantorovich and A. Ivanov, *J. Magn. Magn. Mater.*, 2002, **252**, 244–246.
39 S. Kantorovich, A. O. Ivanov, L. Rovigatti, J. M. Tavares and F. Sciortino, *Phys. Rev. Lett.*, 2013, **110**, 148306.
40 J. J. Weis and D. Levesque, *Phys. Rev. Lett.*, 1993, **71**, 2729–2732.
41 P. J. Camp, J. C. Shelley and G. N. Patey, *Phys. Rev. Lett.*, 2000, **84**, 115–118.
42 S. H. L. Klapp, *J. Phys.: Condens. Matter*, 2005, **17**, R525.
43 P. D. Duncan and P. J. Camp, *Phys. Rev. Lett.*, 2006, **97**, 107202.
44 L. Rovigatti, J. Russo and F. Sciortino, *Phys. Rev. Lett.*, 2011, **107**, 237801.

45 L. Rovigatti, J. Russo and F. Sciortino, *Soft Matter*, 2012, **8**, 6310–6319.
46 A. Sreekumari and P. Ilg, *Phys. Rev. E: Stat., Nonlinear, Soft Matter Phys.*, 2013, **88**, 042315.
47 J. Jordanovic, S. Jäger and S. H. L. Klapp, *Phys. Rev. Lett.*, 2011, **106**, 038301.
48 S. Jäger and S. H. L. Klapp, *Soft Matter*, 2011, **7**, 6606–6616.
49 J. F. Douglas, *Nature*, 2010, **463**, 302–303.
50 B. D. Plouffe, S. K. Murthy and L. H. Lewis, *Rep. Prog. Phys.*, 2015, **78**, 016601.
51 Y. Wu, Z. Wu, X. Lin, Q. He and J. Li, *ACS Nano*, 2012, **6**, 10910–10916.
52 S. Odenbach, *Magnetoviscous effects in ferrofluids*, Springer, 2002.
53 E. De Miguel, L. Rull, M. Chalam and K. Gubbins, *Mol. Phys.*, 1991, **74**, 405–424.
54 M. Schoen and S. H. L. Klapp, *Reviews of Computational Chemistry*, 2007, **24**, 1–517.
55 M. Klokkenburg, B. Erne, J. Meeldijk, A. Wiedenmann, A. Petukhov, R. Pullens and A. Philipse, *Phys. Rev. Lett.*, 2006, **97**, 185702.
56 T. Borbáth, I. Borbáth, S. Günther, O. Marinica, L. Vékás and S. Odenbach, *Smart Mater. Struct.*, 2014, **23**, 055018.
57 D. J. Cleaver, C. M. Care, M. P. Allen and M. P. Neal, *Phys. Rev. E: Stat., Nonlinear, Soft Matter Phys.*, 1996, **54**, 559–567.
58 M. P. Allen and D. J. Tildesley, *Computer Simulation of Liquids*, Oxford University Press, 2006.
59 M. R. Wilson, M. P. Allen, M. A. Warren, A. Suaron and W. Smith, *J. Comput. Chem.*, 1997, **18**, 478–488.
60 P. Bolhuis and D. Frenkel, *J. Chem. Phys.*, 1997, **106**, 666.
61 P. J. Camp, M. P. Allen and A. J. Masters, *J. Chem. Phys.*, 1999, **111**, 9871.
62 J. P. Hansen and I. R. McDonald, *Theory of Simple Liquids*, Academic, London, 2006.
63 P. Ilg and M. Kröger, *Phys. Rev. E: Stat., Nonlinear, Soft Matter Phys.*, 2005, **72**, 031504.
64 M. A. Miller, R. Blaak, C. N. Lumb and J.-P. Hansen, *J. Chem. Phys.*, 2009, **130**, 114507.
65 A. Rahman, *Phys. Rev. [Sect.] A*, 1964, **136**, A405.
66 A. Patti, D. El Marsi, R. van Roij and M. Dijkstra, *Phys. Rev. Lett.*, 2009, **103**, 248304.
67 V. Yannopapas, S. H. L. Klapp and S. D. Peroukidis, *Opt. Mater. Express*, 2016, accepted for publication.

